The Mixing Layer Between Turbulent Fields of Different Scales

S. B. Pope and D. C. Haworth

Sibley School of Mechanical and Aerospace Engineering, Cornell University, Ithaca, New York 14853, USA

Abstract

A modelling study is reported of the interaction and mixing between two semi-infinite homogeneous turbulent flow fields of different scales. This turbulence mixing layer, in which there are no mean velocity gradients, is ideal for studying turbulent energy transport. The velocity joint *pdf* equation is closed by using the Langevin model and is solved by a Monte Carlo method. A novel – and essential – component in the present model is a Lagrangian equation for the dissipation. The model calculations are compared to the experimental data of Veeravalli and Warhaft. There is good agreement between the calculated and measured velocity skewness and excesses, which are the most revealing statistics.

Introduction

A modelling study is reported of the interaction and mixing between two semi-infinite homogeneous turbulent flow fields of different scales. This flow can be (approximately) realized in wind-tunnel experiments by using a turbulence-generating grid with two different bar and mesh sizes. Downstream of the grid, on each side of the mixing layer, there are regions of nearly homogeneous turbulence. The turbulence energies and length scales are different on the two sides, but by careful adjustment of the grid, the mean velocity profile can be made uniform. The subject of the study is the evolution of the turbulence mixing layer that forms between the two fields of homogeneous turbulence. Experiments have been performed by Gilbert [1, 2] and by Veeravalli and Warhaft [3] whose data are compared to the model calculations [1].

The modelling study of this turbulence mixing layer is based on a transport equation for the joint probability density function (*pdf*) of the three components of velocity [4]. The joint *pdf* equation is closed by using the Langevin equation to model the effects of viscosity and the fluctuating pressure gradient, and the resulting modelled *pdf* equation is solved by a Monte Carlo method [5]. A novel feature of the present model is the use of a Lagrangian evolution equation for the dissipation.

The motivation for the study is that in many practical situations a turbulent shear flow is embedded in a surrounding field of turbulence of a different intensity. Examples are: the turbulent buoyant jet from a smoke stack issuing into the atmospheric boundary layer; the dilution jets in a gas turbine combustor issuing into the turbulent flow from the primary zone; and, the boundary layer on a turbine or compressor blade with a turbulent free stream. The flow studied is simpler than these examples and allows the fundamental turbulence phenomena to be examined in a simple geometry and in the absence of shear.

---

[1] It should be noted that the conditions of the experiments reported by Veeravalli and Warhaft in the Symposium Proceedings [3] differ from those reported in this volume. In particular the energy ratios are different. The comparisons made here are with the data reported in the Symposium Proceedings.

In contrast to the flows mentioned above, most laboratory shear flows are surrounded by non-turbulent, irrotational fluid. Then the phenomenon of intermittency is known to be important. Several researchers have argued that turbulence models can be improved by taking excplicit account of intermittency, and have accordingly constructed "conditional models" [6–8]. These conditional models depend upon the fact that the freestream is in a singular state (i.e. zero vorticity) and hence they cannot simply be generalized to treat shear flows in turbulent surroundings. The present study is a first step towards understanding the modelling questions posed by the interaction of turbulence of different scales.

Turbulence Mixing Layer

In a coordinate system moving with the uniform mean flow, the mixing layer in the wind-tunnel experiment is (to a good approximation) statistically one-dimensional and evolves in time. Ideally, this temporally growing mixing layer is as depicted in Fig. 1. In the regions of homogeneity, remote from the mixing layer, the turbulence is isotropic with kinetic energy $k_L(t)$ on the large-scale side ($y > 0$) and $k_S(t)$ on the small-scale side ($y < 0$). The virtual origin of the turbulence is at $t = 0$, and k_L is taken to be unity at $t = 1$. Then with n being the decay exponent, we have

$$k_L(t) = t^{-n}. \tag{1}$$

We take $n = 1.29$, a typical value for grid turbulence. It is assumed that the decay exponent is the same on both sides and so the energy ratio r is constant:

$$r \equiv k_L(t)/k_S(t). \tag{2}$$

In order to make comparisons with Veeravalli and Warhaft's data, we choose the two values of the energy ratio, $r = 7$ and 25.

From the decay equation (1), the dissipation rate is deduced to be

$$\varepsilon_L(t) = -\frac{dk_L}{dt} = nt^{-(n+1)}, \tag{3}$$

and hence the length and time scales are

$$l_L \equiv k_L^{3/2}/\varepsilon_L = t^{(1-n/2)}/n, \tag{4}$$

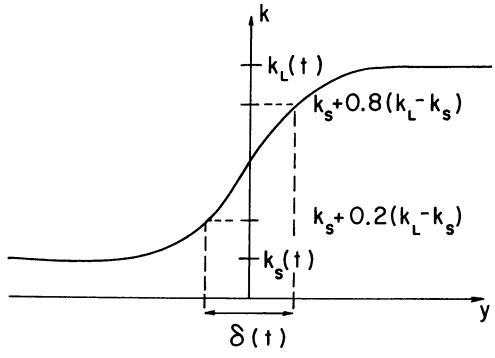

Fig. 1. Sketch of the turbulence mixing layer showing the definition of the thickness δ

and

$$\tau_L \equiv k_L/\varepsilon_L = t/n. \tag{5}$$

On the small-scale side, the dissipation ε_S is smaller by a factor of the energy ratio r, the length scale l_S is smaller by a factor of $\sqrt{r}$, while the time scale is the same.

The virtual origin of the mixing layer is taken to be $t = 1$, at which time the kinetic energy has a step change at $y = 0$. As time evolves, the thickness of the layer $\delta(t)$ (defined on Fig. 1) increases, and statistical quantities develop smooth profiles.

All components of the mean velocity are zero. The mean momentum equation in the y-direction reveals that there is a mean pressure gradient

$$\frac{\partial \langle p \rangle}{\partial y} = -\varrho \frac{\partial \langle v^2 \rangle}{\partial y}, \tag{6}$$

where ϱ is the constant density.

Of primary interest are the profiles of the Reynolds stresses. The turbulence is axisymmetric in the $x - z$ plane (normal to the y-direction): hence the normal stresses $\langle u^2 \rangle$ and $\langle w^2 \rangle$ are equal, and all the shear stresses are zero. But the profile of $\langle v^2 \rangle$ may differ from those of $\langle u^2 \rangle$ and $\langle w^2 \rangle$.

It is possible that the turbulence mixing layer becomes self-similar. Then, all statistical quantities, when normalized by l_L and u_L

$$u_L \equiv (\tfrac{2}{3} k_L)^{1/2}, \tag{7}$$

vary only with the normalized lateral distance η

$$\eta \equiv y/l_L, \tag{8}$$

independent of time. In the experiments [3], the initial conditions for the mixing layer are not easily defined. But it is plausible that the self-similar state has been reached by the last measurement station. Consequently our attention is focussed on this self-similar region, even though the transient model equations are solved, and comparison is made with the state at earlier measurement stations.

Joint *pdf* Model

A Lagrangian viewpoint is useful when modelling, interpreting, and solving *pdf* evolution equations [5]: the behavior of fluid particles in a turbulent flow provides a complete description of the turbulence. At time t, the position and velocity of a fluid particle are denoted by $\hat{\boldsymbol{x}}(t)$ and $\hat{\boldsymbol{u}}(t)$. According to the Navier-Stokes equations, in an infinitesimal time interval dt, $\hat{\boldsymbol{x}}(t)$ and $\hat{\boldsymbol{u}}(t)$ change

$$d\hat{x}_i = \hat{u}_i(t)\, dt, \tag{9}$$

and

$$d\hat{u}_i = -\frac{1}{\varrho}\frac{\partial \langle p \rangle}{\partial x_i} dt + \left(\nu \nabla^2 u_i - \frac{1}{\varrho}\frac{\partial p'}{\partial x_i}\right) dt, \tag{10}$$

where ν is the kinematic viscosity. The Eulerian pressure $p(\boldsymbol{x}, t)$ has been decomposed into

its mean $\langle p \rangle$ and fluctuation $p'(\boldsymbol{x}, t)$. (Angled brackets denote means.) The terms on the right-hand side of (10) are evaluated at the particle location $\boldsymbol{x} = \hat{\boldsymbol{x}}(t)$.

In place of the exact expression (10), we model the Lagrangian velocity increment by the Langevin equation [5, 9, 10]:

$$d\hat{u}_i = -\frac{1}{\varrho}\frac{\partial \langle p \rangle}{\partial x_i}\,dt - \left(\frac{1}{2} + \frac{3}{4}C_0\right)\hat{u}_i\frac{dt}{\tau} + (C_0\hat{\varepsilon})^{1/2}\,dW_i. \tag{11}$$

Here $\hat{\varepsilon}$ is the dissipation associated with the fluid particle (defined below), $\boldsymbol{W}(t)$ is an isotropic Weiner process, and C_0 is a positive constant. The time scale $\tau(\boldsymbol{x}, t)$ is defined by

$$\tau \equiv k/\varepsilon, \tag{12}$$

where ε is the mean dissipation rate

$$\varepsilon(\boldsymbol{x}, t) = \langle \hat{\varepsilon}(t) \,|\, \hat{\boldsymbol{x}}(t) = \boldsymbol{x} \rangle. \tag{13}$$

(For homogeneous turbulence, $\hat{\varepsilon}$ is equal to ε, and the Langevin equation (11) reverts to the standard form used previously [10, 11].)

By comparing (10) and (11) it may be seen that the effects of viscosity and the fluctuating pressure gradient are modelled by the last two terms in (11). The final term represents a random walk in velocity space: $d\boldsymbol{W}$ is a joint normal random vector with zero mean and covariance

$$\langle dW_i dW_j \rangle = dt\,\delta_{ij}. \tag{14}$$

The form of this term is consistent with Kolmogorov inertial-range scaling [12] and the Kolmogorov constant C_0 has been determined to be 2.1 [11].

The penultimate term in (11) represents a linear return to zero velocity fluctuations. For isotropic turbulence, the precise form of the term is completely determined by the condition that the expected energy decays at the rate $\hat{\varepsilon}$. Haworth and Pope [10, 13] have developed and used a generalization of (11) that is applicable to anisotropic turbulence and to inhomogeneous flows with mean velocity gradients. In the generalized model the linear term is more involved although it reduces to the isotropic form in the appropriate limit. The isotropic form is deemed adequate for the turbulence mixing layer since there are no mean velocity gradients, and departures from isotropy are not large.

Boundary conditions for $\hat{\boldsymbol{u}}$ are simply specified: on each side of the mixing layer $\hat{u}_i$ is an isotropic normal random variable with mean zero and variance $2/3\,k_L$ on the large-scale side and $2/3\,k_S$ on the small-scale side.

In the context of the turbulence mixing layer, one aspect of the modelling should be emphasized. Pressure fluctuations have two effects on the Reynolds stresses: they redistribute the energy among the components; and, they can cause transport of energy in physical space. The Langevin equation models the first of these processes, but the second is neglected. Whether the (neglected) energy flux $\langle \boldsymbol{u}p'/\varrho \rangle$ due to pressure fluctuations is significant compared to the convective flux $\langle \boldsymbol{u}(1/2\,\boldsymbol{u}\cdot\boldsymbol{u}) \rangle$ is not known with certainty. One promise of experiments on the turbulence mixing layer is to answer this question.

Dissipation Model

In contrast to previous studies using the Langevin equation, here we use a particle-dependent dissipation rate $\hat{\varepsilon}$ rather than the local mean dissipation ε. This is motivated by

the observations that the mean dissipation rate changes by a factor of the energy ratio r (7, say) across the layer, and that (at least at early times) a fluid particle can traverse the layer in a time interval that is short compared to the turbulent time scale τ. Thus a packet of turbulent fluid (of size l_L) can travel from the large-scale side (where the dissipation is ε_L) to the small scale side (where the dissipation is $\varepsilon_S = \varepsilon_L/r$) more rapidly than the turbulence within the packet can respond to its changed surroundings. For a fluid particle within this packet, the appropriate dissipation rate for use in the Langevin model is closer to ε_L than to the local mean on the small-scale side, ε_S.

In order to account for these phenomena, we use a simple relaxation equation for $\hat{\varepsilon}$:

$$\frac{d\hat{\varepsilon}}{dt} = -C_{\varepsilon 3}(\hat{\varepsilon} - \varepsilon)/\tau - C_{\varepsilon 2}\hat{\varepsilon}/\tau, \tag{15}$$

with boundary conditions $\hat{\varepsilon}(t) = \varepsilon_L(t)$ and $\hat{\varepsilon}(t) = \varepsilon_S(t)$ on the large-scale and small-scale sides. Away from the mixing layer, in the regions of uniformity, $\hat{\varepsilon}$ is equal to ε and hence the first term on the right-hand side of (15) is zero. Then the equation reduces to the standard model equation for ε [14] which, with $C_{\varepsilon 2} = 1 + 1/n$, is consistent with the decay law, (1). Within the turbulence mixing layer, the first term on the right-hand side of (15) causes $\hat{\varepsilon}$ to relax to the local mean value ε at a rate determined by the local time scale τ and the constant $C_{\varepsilon 3}$.

In the next section we report results of the calculations with three different choices of $C_{\varepsilon 3}$: 0, 1/4 and ∞. With the extreme value $C_{\varepsilon 3} = \infty$, $\hat{\varepsilon}$ adopts its local mean value; whereas with the other extreme value $C_{\varepsilon 3} = 0$, $\hat{\varepsilon}$ is equal to ε_L or ε_S depending upon whether the fluid particle originated from the large-scale or small-scale side of the layer. The comparison of calculations with Veeravalli and Warhaft's data suggests that the appropriate value of $C_{\varepsilon 3}$ is about 1/4.

For each fluid particle, $\hat{\varepsilon}(t)$ can be interpreted as the mean dissipation, conditional upon the particle's history $\hat{x}(t)$.

We introduce the Eulerian joint *pdf* of velocity and dissipation, $f(\boldsymbol{V}, \tilde{\varepsilon}; \boldsymbol{x}, t)$. In terms of particle properties, this is the joint probability density of the events $\hat{\boldsymbol{u}}(t) = \boldsymbol{V}$ and $\hat{\varepsilon}(t) = \tilde{\varepsilon}$, conditional upon $\hat{\boldsymbol{x}}(t) = \boldsymbol{x}$. From (11) and (15), we deduce the evolution equation for $f(\boldsymbol{V}, \tilde{\varepsilon}; \boldsymbol{x}, t)$ to be

$$\frac{\partial f}{\partial t} + V_i \frac{\partial f}{\partial x_i} = \frac{\partial}{\partial V_i}\left\{\frac{f}{\varrho}\frac{\partial \langle p\rangle}{\partial x_i} + \left(\frac{1}{2} + \frac{3}{4}C_0\right) f \frac{V_i}{\tau}\right\} + \frac{1}{2} C_0 \tilde{\varepsilon} \frac{\partial^2 f}{\partial V_i \partial V_i}$$
$$+ \frac{1}{\tau}\frac{\partial}{\partial \tilde{\varepsilon}}\{f[C_{\varepsilon 3}(\tilde{\varepsilon} - \varepsilon) + C_{\varepsilon 2}\tilde{\varepsilon}]\}. \tag{16}$$

This joint *pdf* equation was solved by a Monte Carlo method [5]. For the flow considered, the method amounts to solving (11) and (15) for a large number ($\approx$ 20,000) of notional particles.

Results

We report, first, results for the energy ratio of 7 (corresponding approximately to Veeravalli and Warhaft's 3:1 grid) with the model constant $C_{\varepsilon 3} = 1/4$. Then the influence of the constant $C_{\varepsilon 3}$ is demonstrated by results obtained with the extreme values $C_{\varepsilon 3} = 0$ and $C_{\varepsilon 3} = \infty$. Finally some results are reported for the energy ratio 25, corresponding approximately to the 7:1 grid.

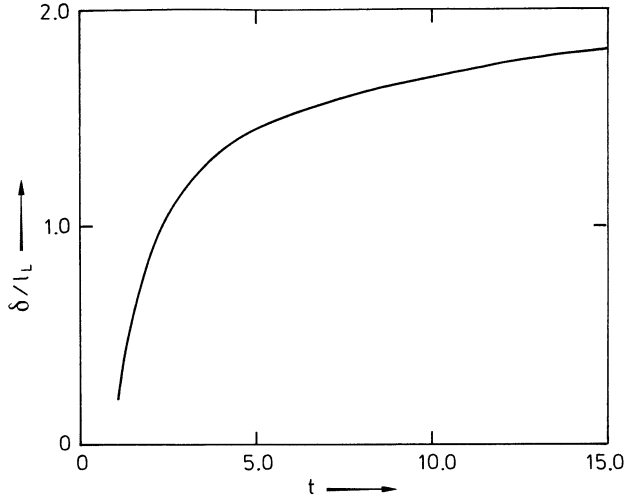

Fig. 2. Calculated evolution of normalized thickness ($r = 7$, $C_{\varepsilon 3} = 1/4$)

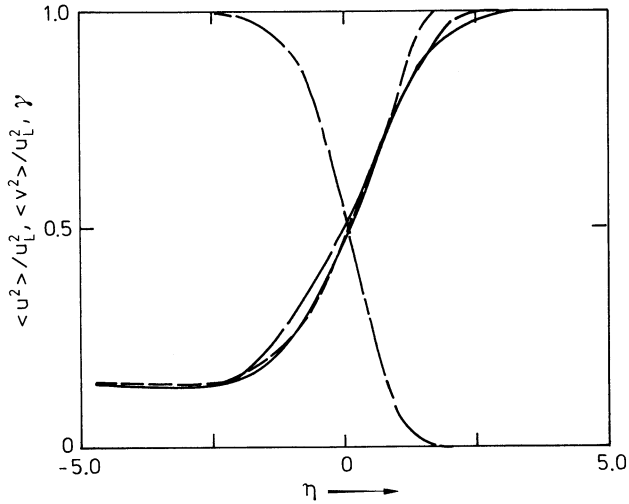

Fig. 3. Calculated normalized variances and intermittency profiles ($r = 7$, $C_{\varepsilon 3} = 1/4$, $t = 15$). ----- $\langle u^2 \rangle$; — — — $\langle v^2 \rangle$; —— error function; — - — γ

For the energy ratio $r = 7$ and $C_{\varepsilon 3} = 1/4$, Fig. 2 shows the temporal growth of the mixing layer: the thickness $\delta(t)$ (defined on Fig. 1) is normalized by $l_L(t)$. It may be seen that an asymptotic value of $\delta/l_L \approx 1.9$ is being approached, but the asymptote is not quite attained by the end of the calculations ($t = 15$).

In Fig. 3, the variances $\langle u^2 \rangle$ and $\langle v^2 \rangle$ at $t = 15$ (normalized by u_L) are plotted against the normalized cross-stream coordinate η (8). An error function curve (with the same maximum slope as $\langle u^2 \rangle / u_L^2$) is shown for comparison. It may be seen that the $\langle u^2 \rangle$ profile differs significantly from the error function on the large-scale side. The calculated spread of the $\langle v^2 \rangle$ profile is slightly greater than that of $\langle u^2 \rangle$.

Also shown in Fig. 3 is the "intermittency factor" γ, defined to be the probability of the fluid having come from the small-scale side.

In performing calculations with different values of $C_{\varepsilon 3}$ and different energy ratios r, we found that the spreading rate and the variance profiles changed little. The most sensi-

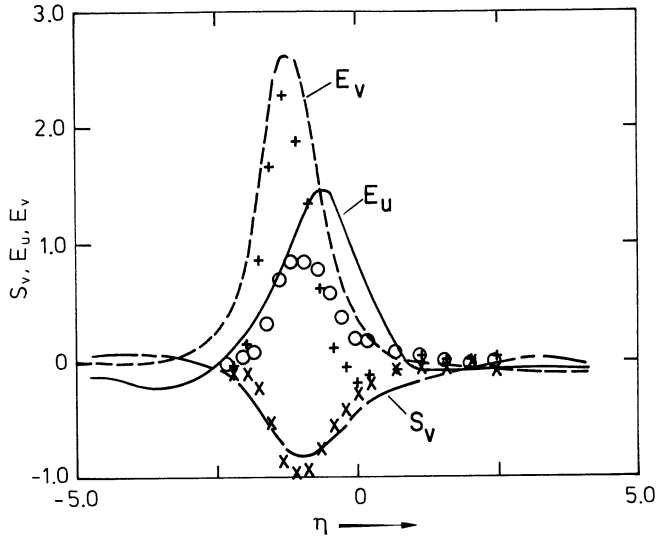

Fig. 4. Excesses of u and v and skewness of v. Lines are calculations ($r = 7$, $C_{\varepsilon 3} = 1/4$, $t = 15$), symbols are experimental data of Veeravalli and Warhaft (3:1 grid, $x = 150$ cm)

tive quantities were the excesses E_u and E_v ($E_u \equiv \langle u^4 \rangle / \langle u^2 \rangle^2 - 3$) and the skewness ($S_v \equiv \langle v^3 \rangle / \langle v^2 \rangle^{3/2}$). (The skewness of u is zero by symmetry.) Figure 4 shows the calculated values of E_u, E_v and S_v at $t = 15$ compared to the measurements at the furthest measurement station ($x = 150$ cm). It may be seen that both in shape and magnitude the calculations are in good agreement with the measurements. The peaks in all the profiles are significantly displaced towards the small-scale side, with the peak of E_v being further out than that of E_u. (It should be noted that the cross stream coordinate has not been normalized by the width of the layer, nor has the origin been shifted.) The measured peak value of E_v is 2.3 and that calculated is 2.5. On the other hand, with $C_{\varepsilon 3} = 0$ and $C_{\varepsilon 3} = \infty$, the calculated values are 3.2 and 0.8, respectively. The intermediate value $C_{\varepsilon 3} = 1/4$ was chosen to give approximately correct peak values of E_u, E_v and S_v at this location.

The measurements at the upstream station ($x = 45$) clearly show that self-similarity has not been attained at that location (see Fig. 6a of [3]): the magnitudes of the excesses and skewness are higher than at the downstream station. In the calculations too these magnitudes decrease with time. But there is no unambiguous means of determining the appropriate time t at which to compare calculations with the measurements at $x = 45$ cm. In Fig. 5 the calculated profiles of E_u, E_v and S_v at $t = 6$ are compared to those measured at $x = 45$ cm. This time ($t = 6$) was chosen for the comparison because the peak values were in general agreement. Again, in shape and magnitude there is good agreement between calculations and measurements. The agreement would be improved if the width of the calculated layer were slightly greater, and hence the calculated profiles were shifted slightly to the left.

The fundamental effect of different values of $C_{\varepsilon 3}$ is most evident in the conditional variances. We define $\langle u^2 \rangle_s$ and $\langle u^2 \rangle_l$ to be the variances of u conditional upon the fluid having originated on the small-scale and large-scale sides respectively. Figure 6 shows $\langle u^2 \rangle_s$ plotted against the unconditional variance $\langle u^2 \rangle$ for the three values of $C_{\varepsilon 3}$: 0, 1/4 and ∞. With $C_{\varepsilon 3} = 0$, the dissipation $\hat{\varepsilon}(t)$ of all fluid particles originating from the small-scale side is $\varepsilon_s(t)$, irrespective of the particle location $\hat{\boldsymbol{x}}(t)$. Consequently the conditional variance $\langle u^2 \rangle_s$ is almost independent of position (and hence of $\langle u^2 \rangle$). (There is a small dependence on

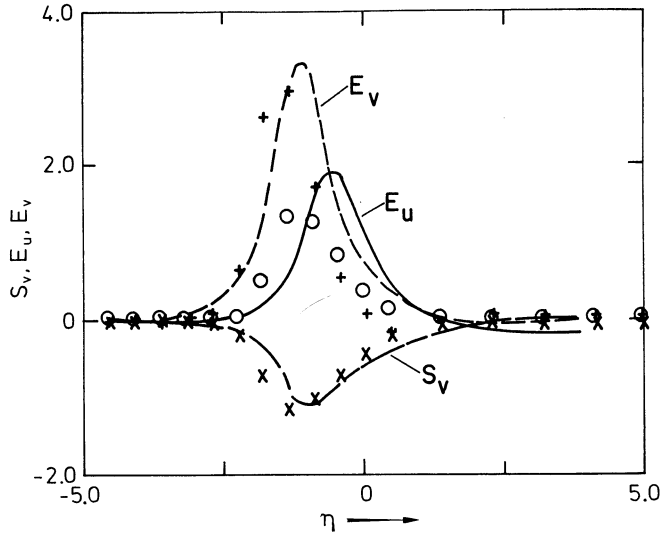

Fig. 5. Excesses of u and v and skewness of v. Lines are calculations ($r = 7$, $C_{\varepsilon 3} = 1/4$, $t = 6$), symbols are experimental data of Veeravalli and Warhaft (3:1 grid, $x = 45$ cm)

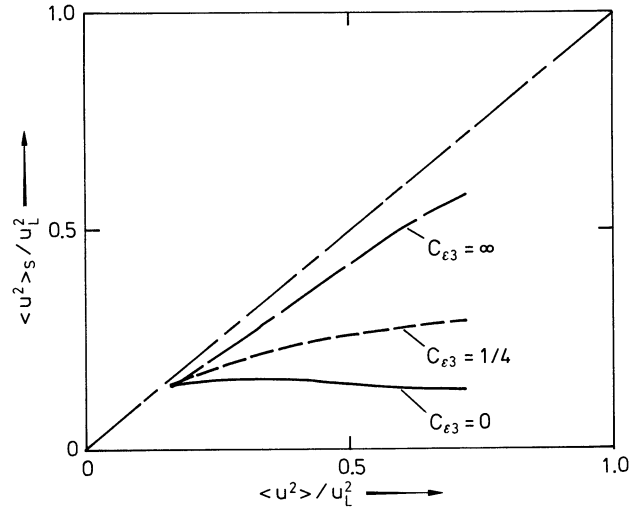

Fig. 6. Calculated variances of u, conditional on the fluid having originated on the small-scale side, against the unconditional variance ($r = 7$, $t = 15$, $C_{\varepsilon 3} = 0, 1/4, \infty$)

position because the time scale τ varies across the mixing layer, even though it has the same value in both uniform streams.) At the opposite extreme, with $C_{\varepsilon 3} = \infty$, the particle dissipation $\hat{\varepsilon}(t)$ is always equal to the local mean ε. These fluid particles rapidly lose the influence of their origin and the conditional variance $\langle u^2 \rangle_s$ is close to the unconditional variance $\langle u^2 \rangle$. With the intermediate value $C_{\varepsilon 2} = 1/4$, this conditional variance $\langle u^2 \rangle_s$ increases above its boundary value, but is significantly below the value with $C_{\varepsilon 3} = \infty$.

We now consider Veeravalli and Warhaft's data for the 7:1 grid. In the experiment, because the uniform streams are not completely isotropic, the variance ratios $\langle u^2 \rangle_L / \langle u^2 \rangle_s = 30$ and $\langle v^2 \rangle_L / \langle v^2 \rangle_S = 22$ are not the same. In order to make comparisons

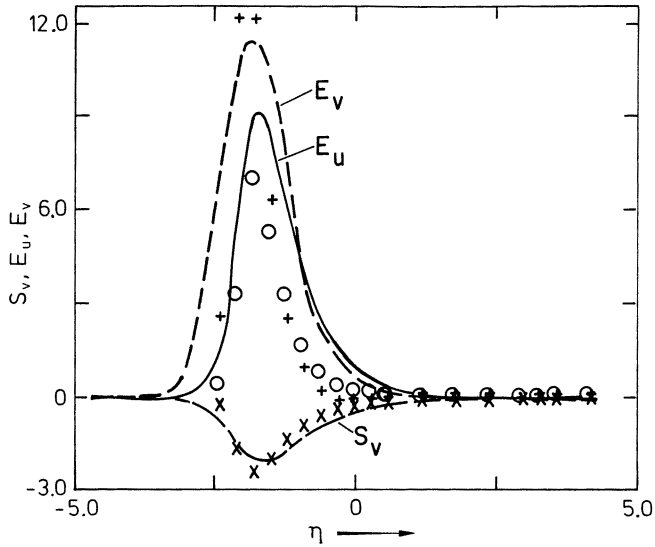

Fig. 7. Excesses of u and v and skewness of v. Lines are calculations ($r = 25$, $C_{\varepsilon 3} = 1/4$, $t = 15$), symbols are experimental data of Veeravalli and Warhaft (7:1 grid, $x = 62$ cm)

with these data, we made calculations with the energy ratio $r = 25$ (and with isotropic streams). Since the one new model constant $C_{\varepsilon 3}$ was chosen by reference to the 3:1 grid data, the following calculations can, to an extent, be regarded as predictions.

Figure 7 shows the calculated excesses and skewness at $t = 15$ compared to Veeravalli and Warhaft's 7:1 grid data at the single measurement station $x = 62$ cm. (It is not known whether self-similarity has been attained at this location.) The shapes of the curves and their relative positions are similar to the 3:1 grid results, but the magnitudes are much greater. The calculated peak excess of v is $E_v = 11.5$ which agrees well with the measured value of 12.1.

Discussion and Conclusion

With the use of a novel Lagrangian equation for dissipation (15), the Langevin model has been successfully applied to the turbulence mixing layer. The most revealing statistics in the flow are the velocity skewness and excesses. These quantities are calculated in good agreement with the data of Veeravalli and Warhaft [3] for both 3:1 and 7:1 grids. The calculated $\langle v^2 \rangle$ profile is slightly wider than the $\langle u^2 \rangle$ profile, but the distinctive measured profile shapes [3] were not observed.

The standard Langevin model, in which the local mean dissipation rate ε is used, is recovered from the present model with the model constant value $C_{\varepsilon 3} = \infty$. Then the particle dissipation $\hat{\varepsilon}$ relaxes instantaneously to the local mean ε. But it is significant that the appropriate value of $C_{\varepsilon 3}$ is quite small ($C_{\varepsilon 3} = 1/4$). This indicates that the relaxation is quite slow and hence the particle's history significantly influences its evolution.

The Lagrangian dissipation equation (15) is stated here for the case of isotropic turbulence with no mean velocity gradients. But the equation is readily generalized and its use in *pdf* calculations of inhomogeneous flow (e.g. [13]) will be investigated.

Further insight into the statistical nature of the dissipation can be found in Kolmogorov's similarity hypotheses of 1962 and their consequences [15]. A refined particle dissipation model based on these considerations is in its early stages of development [16]. The new model replaces (15) with a stochastic diffusion process such that $\hat{\varepsilon}(t)$ has a log-normal distribution.

Until recently, the turbulence mixing layer had not been studied experimentally, and the flow has been ignored by turbulence modellers. It is an extremely interesting flow from which much can be learned. In future experiments it would be useful to include a small temperature difference between the streams. Then, not only could scalar mixing be studied, but temperature could serve as an (imperfect) indicator of the origin of fluid particles. Consequently it would be possible to obtain conditional statistics which reveal a great deal about the processes involved (see Fig. 6, for example).

Acknowledgement. We are grateful to S. Veeravalli and Z. Warhaft for making their preliminary results available to us.

References

1. Gilbert, B. (1980): Diffusion mixing in grid turbulence without mean shear. J. Fluid Mech. **100**, 349–365
2. Gilbert, B. (1976): "An Experimental Investigation of Turbulent Mixing of Fluids with Different Dynamically Significant Scales;" Ph.D. Thesis, University of Illinois at Chicago Circle
3. Veeravalli, S., Warhaft, Z. (1986): "The Interaction of Two Distinct Turbulent Velocity Scales in the Absence of Mean Shear," this volume, p. 21
4. Pope, S. B. (1981): Transport equation for the joint PDF of velocity and scalars in turbulent flow. Phys. Fluids **24**, 588–596
5. Pope, S. B. (1985): PDF methods for turbulent reactive flows. Prog. Energy Combust. Sci. **11**, 119–192
6. Libby, P. A. (1975): On the predicition of intermittent turbulent flows. J. Fluid Mech. **68**, 273–295
7. Byggstoyl, S., Kollmann, W. (1981): Closure model for intermittent turbulent flows. Int. J. Heat Mass Transfer **24**, 1811–1822
8. Pope, S. B. (1984): Calculations of a plane turbulent jet. AIAA J. **22**, 896–904
9. Pope, S. B. (1983): A Lagrangian two-time PDF equation for turbulent flows. Phys. Fluids **26**, 3448–3450
10. Haworth, D. C., Pope, S. B. (1985): A generalized Langevin model for turbulent flows. Phys. Fluids **29**, 387–405
11. Anand, M. S., Pope, S. B. (1984): "Diffusion Behind a Line Source in Grid Turbulence," in *Turbulent Shear Flows 4,* ed. by L. J. S. Bradbury et al. (Springer, Berlin, Heidelberg), pp. 46–61
12. Obukhov, A. M. (1959): Description of turbulence in terms of Lagrangian variables. Adv. Geophys. **6**, 113–116
13. Haworth, D. C., Pope, S. B. (1985): "Application of a Generalized Langevin Model to the Two-Dimensional Mixing Layer," Fifth Symposium on Turbulent Shear Flows, Cornell University
14. Launder, B. E., Spalding, D. B. (1972): *Mathematical Models of Turbulence,* (Academic, New York)
15. Monin, A. S., Yaglom, A. M. (1975): *Statistical Fluid Mechanics,* Vol. 2, (MIT Press, Cambridge)
16. Haworth, D. C., Pope, S. B. (1985): "Langrangian dissipation models for turbulent flows," Bull. Am. Phys. Soc. **30**, 1694